



# Passive Blowing Strategy to Enhance Aerodynamic Performance and Noise of a Hollow-bladed Axial Fan: An Experimental Study

A. Bouanik<sup>1,2,3†</sup>, T. Azzam<sup>2</sup>, A. Larabi<sup>2</sup>, A. Mammeri<sup>3,4</sup>, M. Mekadem<sup>2</sup> and F. Bakir<sup>3</sup>

<sup>1</sup> *Research Laboratory in Energetics, Flows and Transfers, Military Academy of Cherchell, Tipaza, 42067, Algeria*

<sup>2</sup> *Laboratory of Fluid Mechanics, Military Polytechnical school, Bordj El Bahri, Algiers, 16046, Algeria*

<sup>3</sup> *Arts et Métiers Institute of Technology, CNAM, LIFSE, HESAM University, Paris, 75013, France*

<sup>4</sup> *Valeo Thermal Systems, La Verriere, 78320, France*

†Corresponding Author Email: [d\\_bouanik.ayoub@emp.mdn.dz](mailto:d_bouanik.ayoub@emp.mdn.dz)

## ABSTRACT

This research explores the efficacy of a passive control strategy designed to enhance the performance of an axial hollow fan. This investigation uses a dedicated experimental setup to evaluate various aspects of the fan's performance, including characteristics, efficiency, acoustic emissions, and flow topology. The control strategy involves introducing a portion of the main flow into the hollow fan through an upstream opening in the hub. Capitalizing on centrifugal forces, this air portion is injected into the fan's periphery via an axial slot at the rotating shroud ring. Additionally, to refine the previous strategy, a centrifugal fan is incorporated into the hub to assist in directing the flow toward the hollow blades and effectively overcoming losses. The study's findings reveal that implementing this control strategy broadens the fan's operating range and shifts its optimal operating point towards higher flow rates. This improvement is accompanied by a substantial increase in the fan's power density. Furthermore, a notable reduction in sound emissions of approximately 3 dB was recorded, especially when employing the centrifugal fan in the hub. This control strategy also significantly modifies the flow topology downstream of the fan, shifting it from an axial direction to a radial one.

## Article History

Received February 16, 2024

Revised April 20, 2024

Accepted May 2, 2024

Available online July 13, 2024

## Keywords:

Passive control  
Passive injection  
Axial fan  
Centrifugal fan  
Hollow fan  
Slot

## 1. INTRODUCTION

In the contemporary era, technological advancements are prominent, driving continuous evolution across industries, notably in sectors such as automotive, navy, and the rapidly advancing field of artificial intelligence, which necessitates efficient processing of vast amounts of data using robust computing systems. Particularly in these domains, systems are renowned for generating elevated temperatures. Underscoring the critical need to develop efficient thermal management systems to address temperature-related challenges. Typically, such systems incorporate fans to mitigate heat and ensure optimal performance.

Within this framework, a primary research objective is to improve the effectiveness of these fans in terms of both the power they deliver and the airflow they produce. Additionally, there is a growing emphasis on reducing noise in these cooling systems. Aligning with the overarching goal of improving aerodynamic performance. This emphasis on noise reduction is especially pertinent

following the widespread adoption of electric vehicles by automotive manufacturers, reflecting a shared commitment to enhance human comfort alongside technological advancements. Which also aligns with broader obligations to meet strict environmental regulations.

Several previous works have focused on improving aerodynamic performance, particularly through flow control methods. Notable contributions include studies by Azzam et al. (2017), Pereira et al. (2021) and Bouanik et al. (2023, 2024), which investigate the effectiveness of active control strategies numerically and experimentally. These studies specifically examine the same hollow fan geometry discussed in the current investigation, along with other axial turbomachinery configurations studied by Neuhaus and Neise (2007), Sheng and Zhao (2017) and Chen et al. (2022).

While active control methods offer potential performance enhancements, they often entail high costs and logistical challenges, particularly in space management within rotating systems. As an alternative,

| NOMENCLATURE |                              |            |  |
|--------------|------------------------------|------------|--|
| $\mu$        | air dynamic viscosity        | LS         | peak correspond to large structures      |
| $c$          | blade's chord length         | $\psi$     | pressure coefficient                     |
| BPF          | Blade Passing Frequency      | $\Delta P$ | pressure difference generated by the fan |
| $c_m$        | mean chord length            | $u_m$      | velocity at the mean radius              |
| $\rho$       | density                      | C          | resistive net torque                     |
| $\Phi$       | flow coefficient             | $\omega$   | rotational speed                         |
| $Q_v$        | flow rate                    | n          | rotation speed                           |
| MFT          | Mixed-Flow Turbomachinery 3D | d          | slot dimension                           |
| B            | number of fan blades         | $T_1$      | gap clearance                            |
| D            | overall fan diameter         | $u$        | tip velocity                             |

researchers are encouraged to explore passive control mechanisms. Noteworthy contributions in this regard include works by Nadeau (2005), Buisson et al. (2013), S. Chen et al. (2017), and L. Chen et al. (2018), focusing on geometrical modifications as a control strategy, as well as passive injection strategies studied by Eberlinc et al. (2009) and Wasilczuk et al. (2021).

Before implementing noise reduction strategies, it is essential to identify the primary sources of sound emission, with aerodynamic phenomena, particularly the interaction between the primary flow and leakage flow through the gap clearance between the fan and casing, being a significant source. Studies by Piellard et al. (2014), Boudet et al. (2015), Magne et al. (2015), Pogorelov et al. (2016), Moreau and Sanjose (2016) and Canepa et al. (2016) offer valuable insights into this interaction and its implications for blade performance.

Efforts to mitigate aerodynamic noise have led to research into flow control methods and blade geometry modifications, exemplified by studies conducted by Qingyi et al. (2023) and Yadegari et al. (2024).

This study focuses on a new generation of axial hollow fans characterized by their lightweight design owing to their hollow structure, resulting in reduced power consumption for rotation. Previous investigations, including those by Azzam et al. (2017), Pereira et al. (2021) and Bouanik et al. (2024), that have demonstrated significant improvements using active control strategies involving rotating air blowing from the shroud ring of the fan. These studies primarily focus on enhancing aerodynamic performance using the hollow part of the fan, directing air through perforated holes and slots in the rotating shroud ring.

The contribution of a passive control strategy was examined numerically for the first time, using the same blowing geometry (slot) discussed in Bouanik et al. (2024), where numerical model and mesh generation were meticulously examined, taking into account the main outcomes from previous investigations such as those by Yadegari and Bak Khoshnevis (2020, 2021). The study resulted in an improvement in aerodynamic performance, leading to a substantial gain in aerodynamic power. The strategy involves exploiting an opening upstream of the hub to guide part of the main flow through the hollow blades, which is then injected from the rotating shroud ring. Additionally, a centrifugal fan has been integrated into the fan's central hub.

In summary, this study presents an experimental investigation into the effectiveness of a passive control strategy previously studied numerically, aiming to enhance aerodynamic performance and flow topology. Unlike complex active control methods, which often require additional energy sources and drive systems, this control strategy prioritizes feasibility and integration into complex systems. It achieves this by promoting self-suction from the main flow through the incorporation of an opening in the upstream side of the hub and integrating a centrifugal fan within it, thereby minimizing the need for additional energy. The strategy uses centrifugal effects to direct the drawn air towards the fan's periphery via its hollow blades, with injection occurring through a 4mm-sized axial slot encircling the fan's entire periphery in the shroud ring.

The advantages and applications of this control strategy to the studied fan are significant, resulting in a reduction in aerodynamic noise and enhanced operation in confined spaces, even at high flow rates. Additionally, the controlled fan delivers significant power density at the same rotation speed, enabling more efficient cooling and higher efficiency in overcoming pressure losses in system circuits, accompanied by an expansion of the fan's operating range and a shift of its highest optimal operating point towards high flow rates.

## 2. EXPERIMENTAL SETUP

### 2.1 Experimental Drive System: Design, Implementation, and Performance Analysis

Experimental tests were conducted using a test bench depicted in (Fig. 1 a and b), constructed in accordance with ISO 5801 standards, International Organization for Standardization (2007). The drive control system consisted of a Maxon motor with a control box. This control box was connected to a computer to regulate the fan's rotation speed. Additionally, a torque meter was mounted on the motor shaft to measure both the flow resistive net torque on the fan's walls and the rotation speed, with an uncertainty of less than 0.1%. To analyze the flow rate across the entire operating range and facilitate the sampling of numerous data points per graph, an IRIS flow rate controller was employed to modify the air inlet section. Additionally, if required, an auxiliary motor is activated to achieve the desired flow rate. This auxiliary motor is driven by a frequency converter to precisely adjust its rotation speed. The flow rate was estimated in accordance with ISO 5801 standards

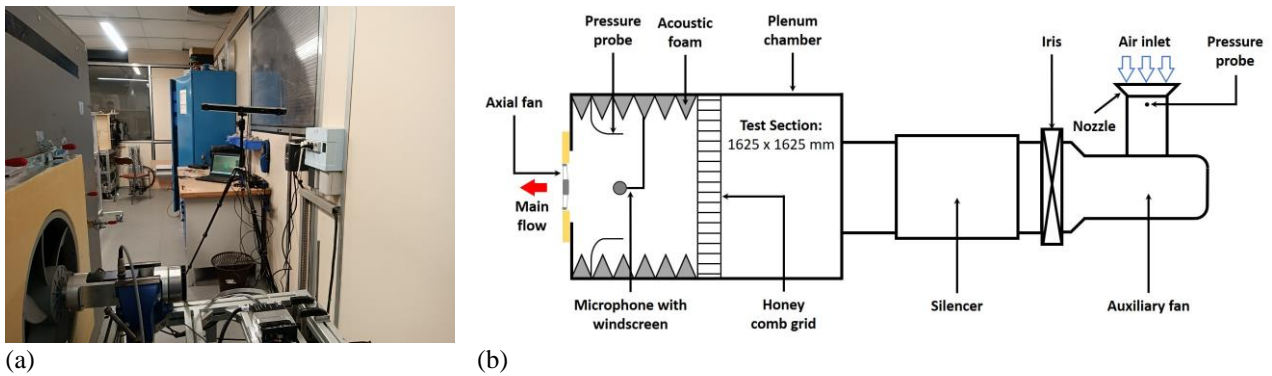


**Fig. 1 Experimental Setup: (a) Experimental Setup for Fan Testing on the Test Bench, using the ProCap 3D Flow Field Measurement System, (b) Plan of the Aeroacoustic Performance Analysis Test Bench**

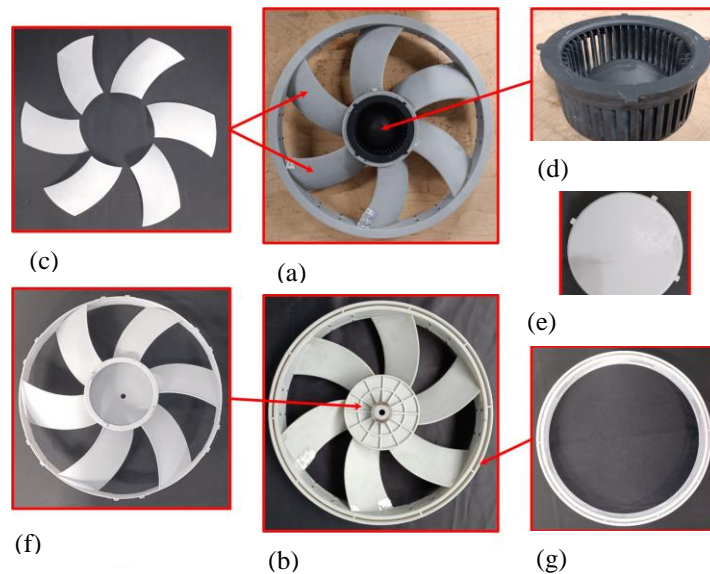


**Fig. 2 Hollow tested fan components: (a) Upstream View of the Complete Tested Fan (Cont-EXP-2 case (Table 1)), (b) Downstream View of the Complete Tested Fan (Cont-EXP-1 and Cont-EXP-2 (Table 1)), (c) Blade's Extrados, (d) Centrifugal Fan (Cont-EXP-2 case (Table 1)), (e) Hub Lid (B-EXP case (Table 1)), (f) Largest Printed Part (Hub, Blade's Intrados, and Shroud's Bottom), (g) Rotating Shroud Ring with Axial Slot**

[International Organization for Standardization \(2007\)](#). This process involved calculating the static pressure at the Air Inlet Nozzle (Fig. 1 b) using sensors positioned on all four sides. These sensors were connected to a Differential Pressure Transmitter. Likewise, pressure measurements within the plenum chamber were acquired using sensors embedded in its four lateral walls, connected to the same Differential Pressure Transmitter. This transmitter ensures measurement accuracy with an uncertainty of less than 0.25% of the reading. Furthermore, a honeycomb was integrated to straighten the flow by breaking the tangential component of speed.

The flow structure was visualized using a "3D Flow Field Measurement System - ProCap by streamwise" (Fig. 1 a), which constitutes a real-time flow visualization system specifically designed to map, process, and present the 3D flow topology directly to the user as the measurement is ongoing. Its essential components include a digital 5-hole flow probe, as used in our case, ensuring a principal precision of less than 0.5% in velocity measurement and less than 1° in flow angle determination. Additionally, it incorporates a tracking camera and an extendable probe pole.

For the acoustic analysis, sound was captured using a strategically placed microphone within the test bench, positioned in front of the fan to measure noise characteristics, as illustrated in (Fig. 1 b). To ensure accurate acoustic analysis, pyramidal-shaped acoustic foam was adhered to all internal surfaces of the plenum chamber, effectively reducing sound wave reflections. Additionally, to minimize noise transmission from the auxiliary motor to the test bench and accurately capture only the sound emitted by the tested fan, a silencer was strategically installed between the auxiliary motor and the plenum chamber. This measure aims to restrict the propagation of unwanted noise, ensuring that the recorded sound exclusively reflects the real performance of the fan under examination.

## 2.2 Tested Fans

This study conducted measurements on an axial fan characterized by a hollow design spanning from the hub to the shroud ring. Incorporating this hollow structure offers benefits such as reduced weight and decreased rotor energy requirements. The fan (as depicted in Fig. 2) was manufactured using a 3D printing process, employing the

Stereolithography (SLA) method. This technique provides the printed fan with a smooth, finely finished surface, a key advantage of this manufacturing method. It was produced in several parts before being assembled to create the final fan under investigation, as depicted in (Fig. 2). Specifically, (Fig. 2 f) represents the most significant printed component, consisting of the blades' intrados connected to the bottom of the shroud ring at the blade's tip and the open hub at the blades' bases.

In the initial assembly step, the extrados are permanently glued to the first part (Fig. 2 f) using high-quality glue, ensuring a robust attachment and excellent airtightness. Furthermore, the rotating shroud ring (Fig. 2 g) is fastened using small screws and nuts to enable smooth interchangeability between shroud rings corresponding to the analyzed cases (outlined in Section 2.3), or for potential adjustments in slot positions in the future. This assembly method aims to streamline production and minimize costs by avoiding printing each fan separately for different cases. Regarding the remaining components, the centrifugal fan (Fig. 2 d) or the lid (Fig. 2 e) are mounted at the upstream side of the hub to complete the final configurations of the studied fan, as depicted in (Fig. 4).

This fan comprises six blades with a blade-tip radius of approximately 179 mm. These blades are interconnected by a rotating shroud ring, enhancing their mechanical strength and resulting in an overall radius of around 195 mm at the fan tip. The hub is 131 mm in diameter, and the blade chord “c” varies from 65 mm to 72 mm, corresponding to the hub and shroud ring, respectively.

The downstream surface of the hub (Fig. 2 b), where the fan is affixed to the motor shaft, has been reinforced to enhance its mechanical strength and structural integrity, ensuring robust support for the fan's weight and rotational speed. Notably, this minor geometric modification has not been previously investigated in numerical studies conducted by (Bouanik et al., 2023) (2024).

It is crucial to emphasize that the studied fan in each configuration underwent a balancing operation (Fig. 3) to mitigate any potential vibrations during testing. The balancing process employed materials provided by Schenck Company.

The centrifugal fan, located within the central hub for the controlled case (Cont-EXP-2), as depicted in (Fig. 3 d), was manufactured using the Stereolithography (SLA) 3D printing process. The geometric design of this centrifugal fan was meticulously crafted through the utilization of the MFT code (Mixed-Flow Turbomachinery 3D), a proprietary software developed in the Laboratory of Fluid Engineering and Energy Systems. This software builds upon the works of two theses authored by Rey (1981) and (Bakir (1992)). It enables a swift and complete approach based on the controlled vortex design method for designing axial and centrifugal compression machines, encompassing both single rotor or rotor-stator stage configurations, facilitating rapid prototyping and performance assessment. The design was based on initial operating conditions in terms of flow rate



**Fig. 3 Experimental Setup: Fan balancing setup for baseline configuration (B-EXP case (Table 1))**

**Table 1 Analyzed scenarios**

| Case       | Description                   |
|------------|-------------------------------|
| B_EXP      | Without control               |
| Cont-EXP-1 | Upstream opened hub           |
| Cont-EXP-2 | Twined axial-centrifugal fans |

“ $Q_v$ ,” total pressure rise “ $\Delta P$ ,” and rotation speed “ $n$ ” extracted from previous studies conducted by our research team.

### 2.3 Control Strategy

In this investigation, the chosen blowing geometry was selected to mirror the configuration studied by Bouanik et al. (2024), ensuring a basis for comparative analysis. The selected slot was positioned in the axial direction, as illustrated in (Fig. 4 d), with a dimension set to ( $d=4$  mm). The selection of the slot dimension (denoted as “ $d$ ”) was initially arbitrary in Bouanik et al. (2024) by establishing a correlation with the gap clearance dimension (denoted as “ $T_1$ ”). Specifically, two scenarios were considered: where ( $d = T_1$ ) and where ( $d = \frac{T_1}{2}$ ). Upon confirmation of the effectiveness of this control strategy, further research will focus on investigating this dimension to determine the optimal configuration in the future.

Two distinct flow control strategies were employed for the current investigation. The first strategy involved creating an opening in the hub on the upstream side (Fig. 4 b) to allow a portion of the main flow to be incorporated into the fan's internal components. This redirected flow was then guided through hollow blades towards the rotating shroud ring under the influence of the centrifugal effect and subsequently injected through the axial slot. The second strategy, illustrated in (Fig. 4 c), entailed

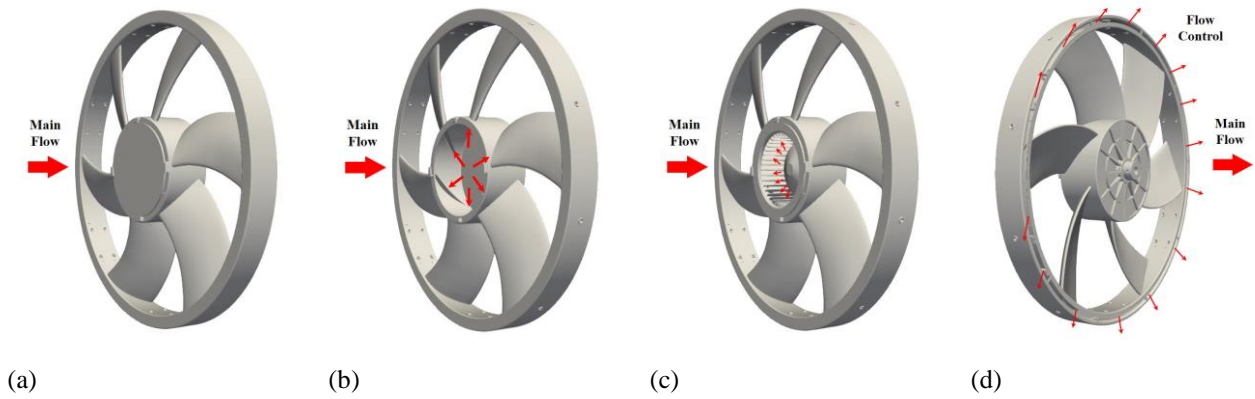


**Fig. 4 The Fan Geometries Examined Across Various Cases. (a) Baseline case, (b) Upstream opened hub strategy, (c) Twined Axial-Centrifugal fans strategy, (d) Downstream view (Flow direction from left to right)**

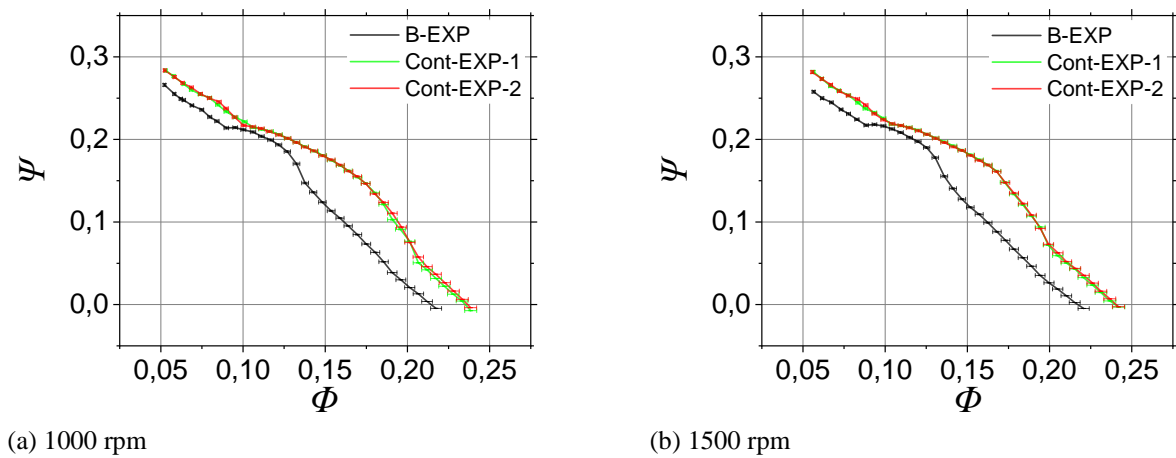


**Fig. 5 Fan characteristics for all tested scenarios**

integrating the designed centrifugal fan (as depicted in Fig. 2 a and d) within the hub. This integration aimed to overcome losses within the fan against the drawn portion of the main flow while enhancing its distribution, orientation, and characteristics within the fan.

To assess the effects of centrifugal forces on this control mechanism, two rotation speeds were tested: 1000 and 1500 rpm. These speeds were selected based on prior research conducted on the same fan geometry by [Azzam et al. \(2017\)](#), [Pereira et al. \(2021\)](#) and [Bouanik et al. \(2024\)](#), facilitating future comparative analyses of the adopted control strategy effectiveness against earlier approaches. Previous studies investigated rotation speeds of 1000, 1500, and 2000 rpm. However, in this study, the 2000 rpm speed was intentionally avoided to prevent any potential damage due to concerns about the fragility of the printed fan. To facilitate a comprehensive comparative study, all scenarios discussed in this investigation are presented in (Table 1).

### 3. RESULTS AND DISCUSSION

#### 3.1 Fan Characteristics

Figures 5 a and b illustrate the fan's characteristics under various scenarios, comparing both controlled and baseline cases. These characteristics are presented as the

pressure coefficient (Eq. 1) as a function of the flow coefficient (Eq. 2). The figures highlight significant performance improvements resulting from the adopted control strategies discussed in this study, namely Cont-EXP-1 and Cont-EXP-2. This enhancement is reflected in the notable increase in power density delivered by the fan in controlled cases compared to baseline ones at the same rotation speed. Furthermore, this improvement results from the dual impact of the control strategy: firstly, by improving air intake from the test bench, and secondly, by minimizing leakage flow within the gap clearance, including related phenomena near the upper blade zone and the shroud ring, which typically diminish blade efficiency in this zone.

The two controlled cases (Cont-EXP-1 and Cont-EXP-2) exhibit close alignment. However, there is a slight shift of up to 2 Pa in pressure between these two cases. It is worth noting that this marginal difference does not stand out significantly compared to the substantial deviations observed in both controlled cases compared to the case without control (B-EXP). Specifically, a shift of approximately 13.12 Pa at a rotation speed of 1000 rpm was observed, increasing to about 34.61 Pa at 1500 rpm.

Furthermore, a noticeable bump appears in the baseline characteristic curve (B-EXP) at lower flow rates, ranging from 0.17 to 0.26 m<sup>3</sup>/s at a rotation speed of 1000

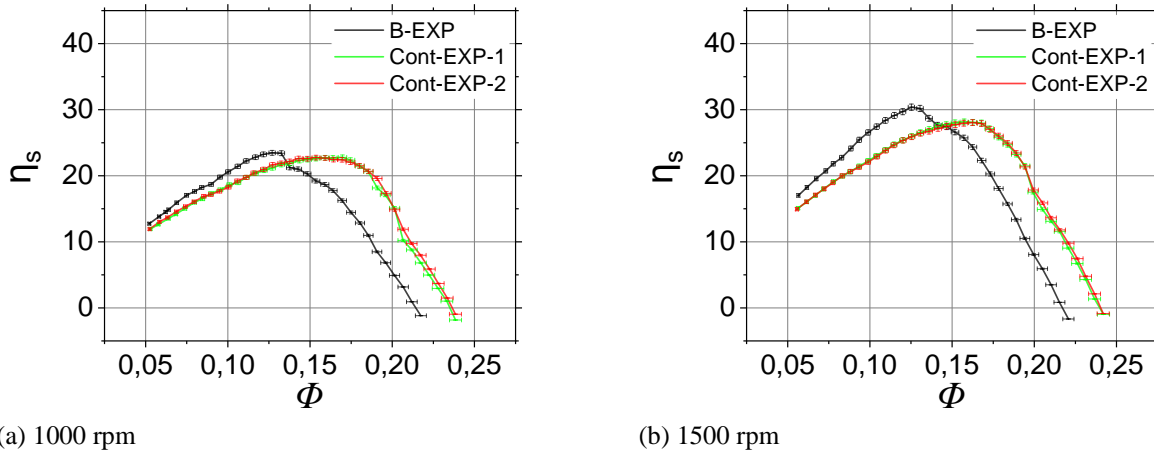


**Fig. 6 Fan efficiency for all adopted strategies**

rpm and from 0.25 to 0.415 m<sup>3</sup>/s at 1500 rpm, corresponding respectively to flow coefficients (Eq. 2) between 0.09 and 0.14 at 1000 rpm and between 0.09 and 0.145 at 1500 rpm. This bump likely contributes to the improvement in fan efficiency within this zone (refer to Section 3.2). The observed bump, resulting from increased power density in the baseline case, notably brings it closer to the controlled case, particularly at flow coefficients of 0.1 for a rotation speed of 1000 rpm and 0.104 for a rotation speed of 1500 rpm. This zone of improvement (bump) is then expanded in controlled cases (Cont-EXP-1 and Cont-EXP-2) to cover most of the operating range, from 0.19 to 0.40 m<sup>3</sup>/s at 1000 rpm and from 0.295 to 0.565 m<sup>3</sup>/s at 1500 rpm, corresponding respectively to flow coefficients between 0.1 and 0.21 at 1000 rpm and between 0.1 and 0.2 at 1500 rpm. However, in the controlled cases, this zone of improvement widens the gap between controlled and baseline cases, notably evident in flow coefficients of 0.175 for a rotation speed of 1000 rpm and 0.168 for a rotation speed of 1500 rpm. According to the authors' knowledge, this bump is likely attributed to a specific characteristic of the studied fan compared to other conventional fans, namely the thick blade nature (approximately 10 mm). For further insights into the choice of blade thickness, refer to the study conducted by Sarraf et al. (2011).

$$\Psi = \frac{2\Delta P}{\rho u^2} \quad (1)$$

$$\Phi = \frac{4Q_v}{(\pi D^2 u)} \quad (2)$$

### 3.2 Fan Efficiency

The fan efficiency, calculated using (Eq. 3), is a crucial decision parameter to consider when assessing fan performances, especially in evaluating the effectiveness of the adopted control strategy in enhancing aerodynamic performance. Figure 6 demonstrates that the applied control tends to broaden the operational range of the fan by approximately 10 % compared to the baseline cases (B-EXP) at both studied rotation speeds, 1000 and 1500 rpm. This expansion is accompanied by a displacement of the nominal operating point towards higher flow rates, exceeding 36 % of the initial operating range (B-EXP) at

the rotation speed of 1000 rpm and over 26 % at 1500 rpm. Additionally, an increase in fan efficiency forming a bump is observed within the same flow rate range discussed in (section 3.1), corresponding to the bump observed in characteristic curves. The maximum efficiency value, initially at 23.5% in the baseline cases (B-EXP), experienced a slight decrease to approximately 22.75% in the controlled cases (both Cont-EXP-1 and Cont-EXP-2) at 1000 rpm, and from 30.4% to 28% at 1500 rpm. It is also observed that throughout the entire range, from the intersection point located at a flow coefficient of 0.14 at 1000 rpm and 0.147 at 1500 rpm up to the highest flow rate, the fan efficiency curve for the controlled cases exhibits a significant increase compared to the curve corresponding to the baseline configuration.

$$\eta_s = \frac{Q_v \Delta P}{C \omega} \quad (3)$$

Much like the fan characteristics, the efficiency of both controlled cases (Cont-EXP-1 and Cont-EXP-2) exhibits close similarity. However, there is a minor deviation of up to 1.7, which is not significantly different when compared to the differences recorded between controlled and baseline cases. These differences were approximately 8.84 at a rotation speed of 1000 rpm and 11.5 at 1500 rpm.

It is also evident that there is a decrease in fan efficiency at 1000 rpm for all studied cases compared to 1500 rpm, likely due to additional losses related to low Reynolds number effects. It is worth noting that the Reynolds numbers for the respective rotation speeds of 1000 rpm and 1500 rpm are  $5.7 \times 10^4$  and  $8.6 \times 10^4$ , respectively, calculated according to (Eq. 4) based on the mean chord length and the velocity at the mean radius.

$$Re = \frac{\rho u_m c_m}{\mu} \quad (4)$$

### 3.3 Aeroacoustics Performances

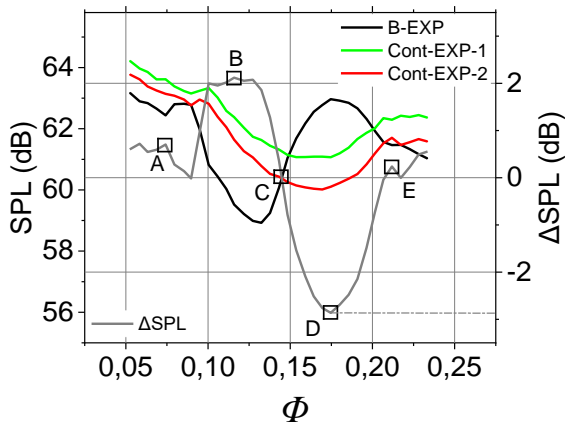
To evaluate the impact of the implemented control strategy on enhancing aeroacoustic characteristics, meticulous preparation of the test bench (as discussed in Section 2.1) was conducted. This preparation ensured high-precision sound calculations, primarily associated with aerodynamic phenomena, especially unsteady ones.

The global sound pressure level obtained for different cases (B-EXP, Cont-EXP-1, and Cont-EXP-2) is presented in Fig. 7 a and b as a function of the flow coefficient. Notably, in each graph, the lowest value of the emitted sound corresponds to the highest efficiency for each case, suggesting that a higher level of stability in flow correlates with increased efficiency. Additionally, the case utilizing the centrifugal fan (Cont-EXP-2) exhibits the most substantial improvement in terms of noise reduction compared to the open hub strategy (Cont-EXP-1) across the entire flow range, prompting us to focus specifically on the former case (Cont-EXP-2) in the subsequent part of this study.

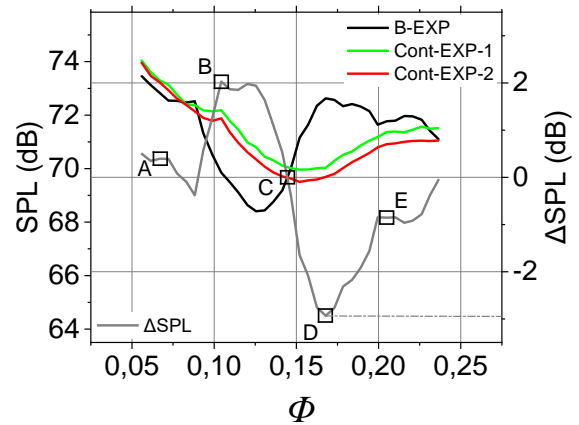
For a more comprehensive analysis, a comparison was conducted between the sound pressure levels emitted in the baseline (B-EXP) and the controlled case (Cont-EXP-2). The difference in globally emitted sound level was calculated using (Eq. 5) and is presented in Fig. 7 a and b, on which points from A to E are designated, forming the focal points of the study on flow structure and acoustic performance comparison. The most significant reduction in the global sound pressure level between the baseline and

controlled cases was observed at a flow rate of 0.33 m<sup>3</sup>/s at 1000 rpm and 0.475 m<sup>3</sup>/s at 1500 rpm, identified as point D. These values correspond to flow coefficients of 0.175 at 1000 rpm and 0.168 at 1500 rpm, respectively. At this juncture, fan performance is optimized, resulting in a maximum reduction in global sound pressure level of approximately 3 dB.

Figures 8, 9 and 10 illustrate the sound pressure level spectrum measurements at points B, C, and D, respectively. The measurements were taken at flow rates of 0.22, 0.27, and 0.33 m<sup>3</sup>/s at the rotation speed of 1000 rpm and 0.295, 0.415, and 0.475 m<sup>3</sup>/s at the rotation speed of 1500 rpm. These flow rates correspond to flow coefficients of 0.116, 0.165, and 0.175 at 1000 rpm and 0.105, 0.147, and 0.168 at 1500 rpm. The figures represent scenarios where the emitted sound pressure level in controlled cases is higher than the baseline (point B), equal to the baseline (point C), and lower than the baseline (point D), respectively. This analysis also provides insights into the variations in sound characteristics under different flow rates and rotation speeds.

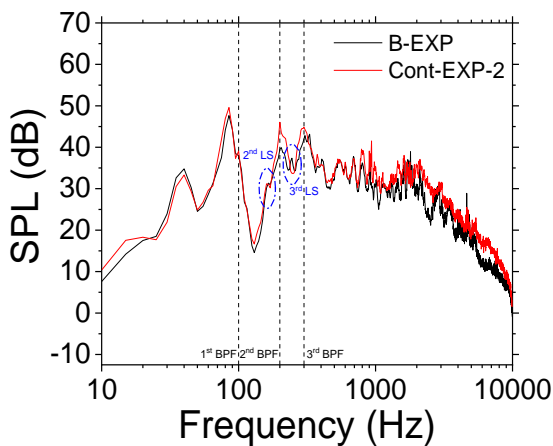


(a) 1000 rpm

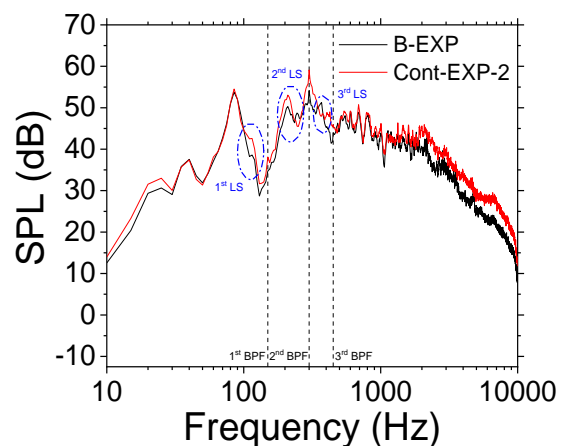


(b) 1500 rpm

**Fig. 7 Sound Pressure Levels for tested scenarios and differences between baseline (B-EXP) and controlled (Cont-EXP\_2) Cases**

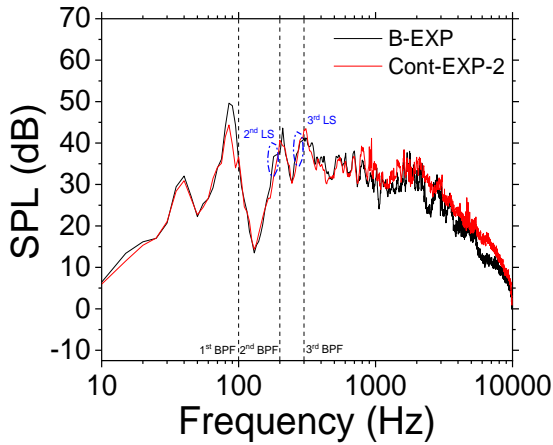


(a) 1000 rpm

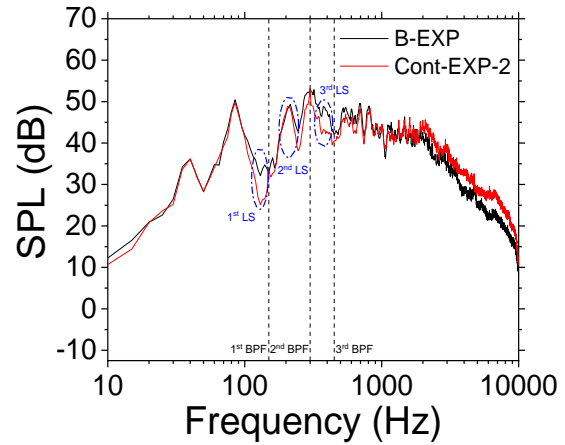


(b) 1500 rpm

**Fig. 8 Sound Pressure Level spectrum registered at point B**

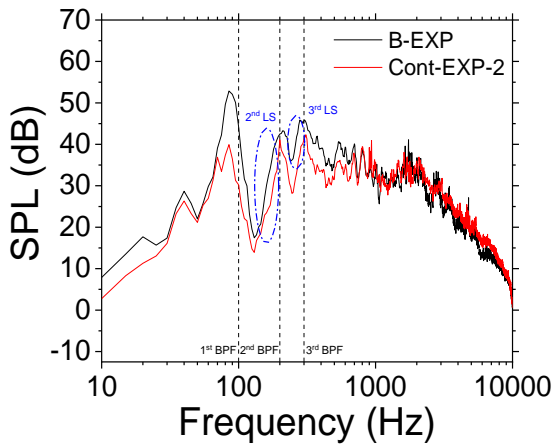


(a) 1000 rpm

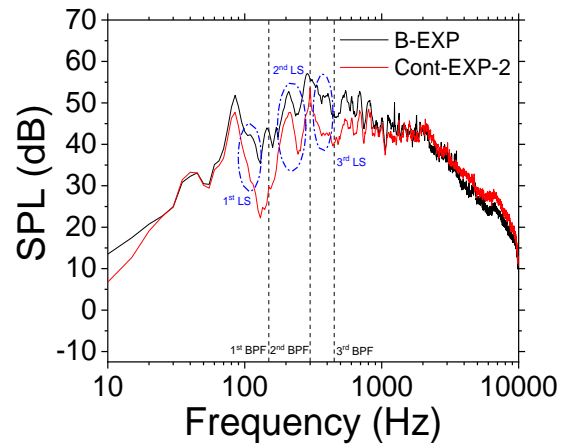


(b) 1500 rpm

**Fig. 9 Sound Pressure Level spectrum registered at point C**



(a) 1000 rpm



(b) 1500 rpm

**Fig. 10 Sound Pressure Level spectrum registered at point D**

Knowing that the significant contribution to the low-frequency noise is originated from phenomena related to the tip leakage flow and unsteady flow structure [Canepa et al., \(2016\)](#). These structures, when re-ingested to the main flow as discussed by [Bouanik et al. \(2024\)](#), impinge upon the rotor blades. Additionally, as highlighted by [Piellard et al. \(2014\)](#), [Magne et al. \(2015\)](#) and [Moreau and Sanjose \(2016\)](#), large structures cause peaks at frequencies slightly lower than the Blade Passing Frequency (BPF) and its harmonics. In (Figs 8, 9, and 10), peaks corresponding to the BPF and others that probably correspond to large structures (denoted as 'LS') are observed and depicted in these figures. Notably, the peak corresponding to the first large structure (1st LS) at 1000 rpm was incorporated into a distinct peak, registering at 85 Hz. It is noteworthy that this particular peak is not directly linked to the rotational speed. At 1500 rpm, large structure peaks are significant, implying that larger structures become increasingly crucial with the increase in rotation speed, as highlighted in studies by [Canepa et al. \(2023\)](#) and [Bouanik et al. \(2024\)](#). The blade passing frequency (BPF) is calculated

using (Eq. 6) and displayed with dashed lines in Figs. 8, 9, and 10, where "B" represents the fan's blade number and "n" is the rotation speed in rpm.

The frequency spectrum in controlled cases further illustrates the effectiveness of the implemented control in noise reduction, up to 13 dB, particularly noticeable at low-frequency noise, especially in the vicinity of peaks corresponding to the blade passing frequency and unsteady phenomena, This reduction may be attributed to the reduction of periodic phenomena associated with the interaction between the main and leakage flows, as discussed by [Canepa et al. \(2021\)](#), and visualized in numerical study by [Bouanik et al. \(2024\)](#). However, at high-frequency noise, a slight difference between baseline and controlled cases is observed; this broadband may be attributed to boundary layer separation on the fan's blades.

$$\Delta SPL = SPL_{Cont-EXP-2} - SPL_{B-EXP} \quad (5)$$

$$BPF = \frac{B n}{60} \quad (6)$$

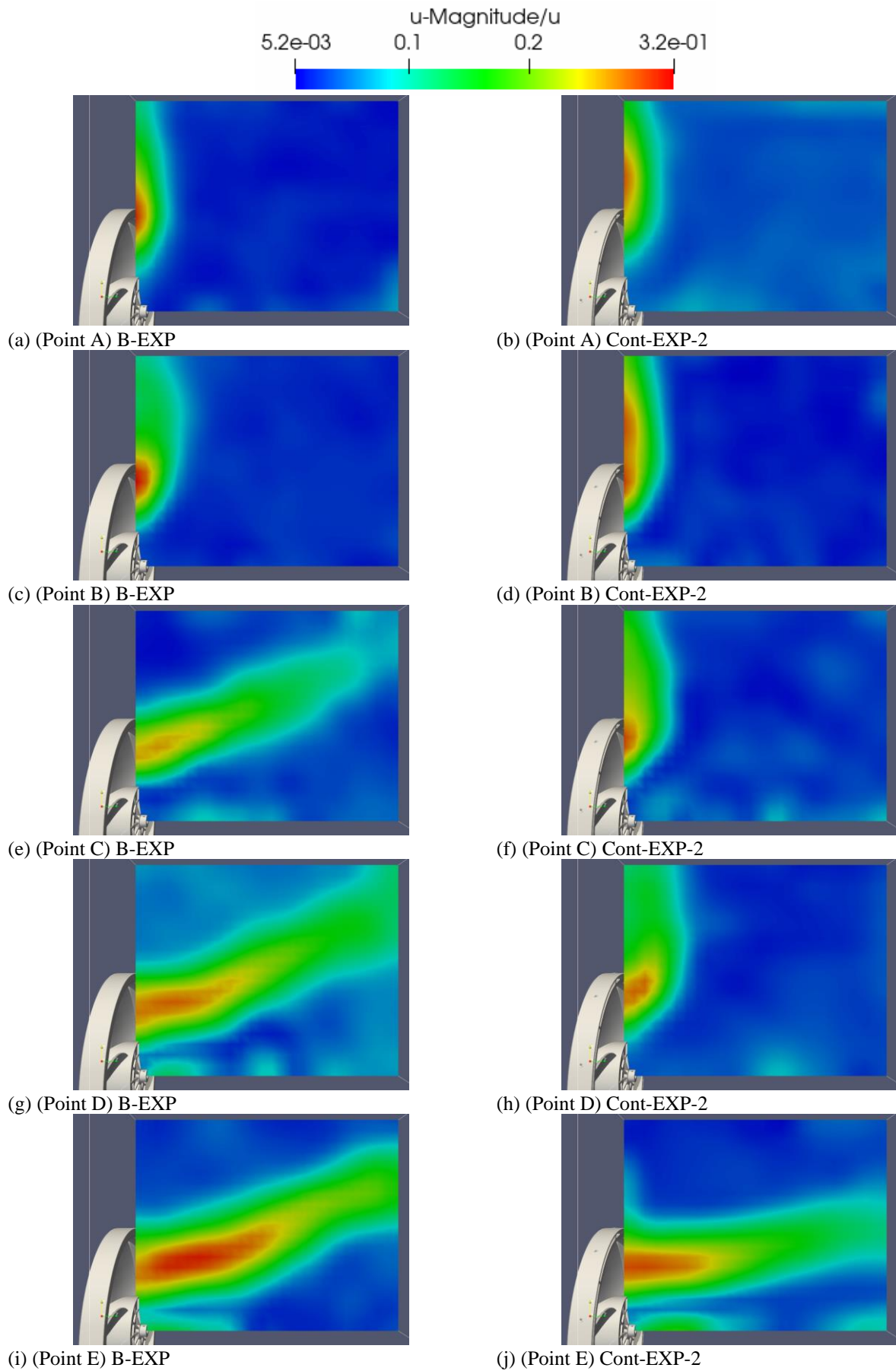


**Fig. 11** Flow structure at rotating speed of 1000 rpm. Left: Baseline cases B-EXP. Right: Controlled cases Cont-EXP-2 (Flow from left to right)

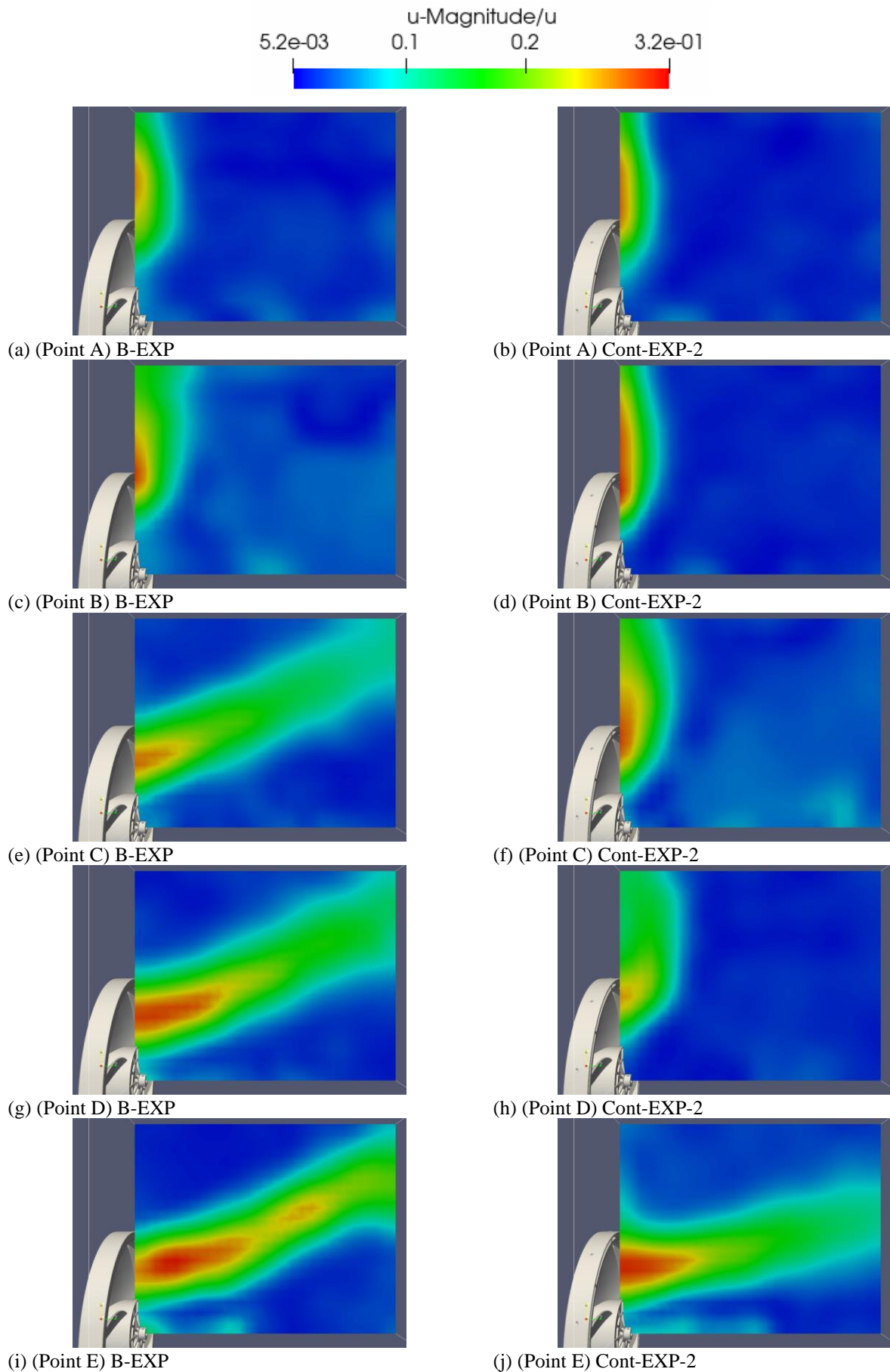


**Fig. 12** Flow structure at rotating speed of 1500 rpm. Left: Baseline cases B-EXP. Right: Controlled cases Cont-EXP-2 (Flow from left to right)

### 3.4 Flow Structure

In this section, we will touch the impact of the adopted control strategy on the flow topology downstream of the fan. Figures 11 and 12 present the velocity magnitude, referred to as “u-magnitude,” for the three velocity components denoted in the ProCap software as “u-x,” “u-y,” and “u-z.” The color map depicted in the figure is divided by the blade tip velocity “u” to facilitate a dimensionless analysis. Notably, the control strategy induces a shift in the flow direction downstream of the fan, transitioning it from an axial direction in the baseline cases to a radial one in the controlled cases, even at high flow rates. Generally, the flow topology in baseline cases at a high flow rate is characterized by its axial configuration at the fan exit (Figs. 11 and 12) (e, g, and i), which shifts to a radial configuration in (Figs. 11 and 12) (f and h) under the adopted flow control effect, while remaining axial towards very high flow rate (Figs. 11 and 12) (i).

We acknowledge that in cases without control, the radial behavior of the fan is commonly observed, particularly when operating at low flow rates, probably due to the blade sweeping effect. In our study, this phenomenon is evident before reaching a flow coefficient of 0.12, as depicted in Figs. 11 and 12 (a and c) for the (B-EXP) case. Notably, this phenomenon is also observed and discussed during numerical studies conducted by Bouanik et al. (2023, 2024), who have associated this shift in flow topology with the formation of a recirculation zone near the rotating shroud ring, which tends to redirect the flow downstream of the fan to the radial direction. The recirculation zone, along with periodic and non-periodic phenomena associated with it, has also been addressed in the works of Canepa et al. (2021).

Furthermore, it is observed that the most significant reduction in sound emission occurs when the flow topology shifts from an axial configuration to a radial one in the controlled cases. This suggests that fewer pressure fluctuations may characterize the radial flow configuration in the controlled cases.

## 4. CONCLUSION

This study explores an experimental approach for implementing passive blowing flow control on an axial fan. In the controlled cases, the approach involves using a perforated slot with a diameter of 4 mm as the blowing geometry; it is positioned on the downstream side of the rotating shroud ring. The injected flow control is drawn from the main flow through an opening in the hub on the upstream side before being transported to the slot via the fan's hollow blades, which act as conduits for the drawn portion of air. Additionally, a centrifugal fan inside the hub may assist in pushing the control flow. The impact of these control strategies on aerodynamic and acoustic performance is comprehensively examined.

In the initial phase of our study, we meticulously analyzed and compared the characteristics and efficiency of the fan in controlled and baseline cases, focusing on two rotation speeds (1000 and 1500 rpm). Our investigation encompassed examining the operating range, identifying the maximum efficiency value, and determining its

position within the flow range. Furthermore, a flow field visualization system conducted a detailed exploration of the flow topology downstream of the fan. Special attention was dedicated to assessing the sound emission, aiming to evaluate the impact of the studied strategy on noise reduction.

The experimental results employing the adopted control strategy reveal a promising enhancement in the fan's performance, affording an additional power density at the same rotational speed. This improvement extends the operating range of the fan by approximately 10 % while shifting the optimal operating point towards higher flow rates, achieving an increase of up to 36 %. Furthermore, there is a noteworthy reduction of global sound emission by about 3 dB, accompanied by a decrease in unsteady phenomena around the fan. The results also indicate a shift in the flow direction downstream of the fan, transitioning from axial to radial orientation.

Furthermore, upcoming efforts will be dedicated to identify the optimal configuration concerning slot dimensions and centrifugal fan design. Additionally, a comprehensive visualization of flow topology near the gap region will be conducted to discern the underlying physics responsible for modifying the flow downstream of the fan. This visualization will be achieved through an in-depth, unsteady numerical study or by employing a Particle Image Velocimetry (PIV) system.

In summary, the control strategy discussed in this investigation offers a broad range of applications for axial fans in industrial settings, even in locations with limited space. Moreover, it promises to enhance acoustic comfort.

## ACKNOWLEDGEMENTS

The investigation was conducted at the LIFSE laboratory in partnership with Valeo Thermal Systems. The authors express their gratitude to Valeo and LIFSE for their invaluable support throughout the research process, with special emphasis on their assistance in conducting the experimental tests. Additionally, we extend our thanks to the IMLET institute for their meticulous language editing and proofreading.

## CONFLICT OF INTEREST

The author declares that there is no conflict of financial or non-financial interest to disclose.

## AUTHORS CONTRIBUTION

**A. Bouanik:** Conceptualization, Data curation, Investigation, Software, Visualization, Formal analysis, Writing – original draft. **T. Azzam:** Conceptualization, Methodology, Software. **A. Larabi:** Methodology, Writing – review & editing. **A. Mammeri:** Visualization, Investigation, Methodology, Resources, Writing – review & editing. **M. Mekadem:** Methodology, Supervision. **F. Bakir:** Conceptualization, Data curation, Resources, Methodology, Validation, Formal Analysis, Data curation, Supervision, Writing – review & editing.

## REFERENCES

- Azzam, T., Paridaens, R., Ravelet, F., Khelladi, S., Oualli, H., & Bakir, F. (2017). Experimental investigation of an actively controlled automotive cooling fan using steady air injection in the leakage gap. *Proceedings of the Institution of Mechanical Engineers, Part A: Journal of Power and Energy*, 231(1), 59–67. <https://doi.org/10.1177/0957650916688120>
- Bakir, F. (1992). *Méthode de dimensionnement et d'analyse des machines de compression hélico-centrifuges en régime incompressible*. Paris, ENSAM.
- Bouanik, A., Azzam, T., Abbasnezhad, N., Larabi, A., Mekadem, M., & Bakir, F. (2024). Active air injection control to enhance performance of hollow-bladed axial fan: a numerical study. *Journal of Applied Fluid Mechanics*, 17(3), 519–533. <https://doi.org/10.47176/jafm.17.3.2201>
- Bouanik, A., Larabi, A., Azzam, T., Mekadem, M., & Bakir, F. (2023). *Experimental and numerical investigation of controlled rotomolded axial fan by internal air injection at gap clearance*. Proceedings of the 9th World Congress on Mechanical, Chemical, and Material Engineering (MCM'23), 1–11. <https://doi.org/10.11159/hfff23.125>
- Boudet, J., Cahuzac, A., Kausche, P., & Jacob, M. C. (2015). Zonal large-eddy simulation of a fan tip-clearance flow, with evidence of vortex wandering. *Journal of Turbomachinery*, 137(6), 1–9. <https://doi.org/10.1115/1.4028668>
- Buisson, M., Ferrand, P., Soulat, L., Aubert, S., Moreau, S., Rambeau, C., & Henner, M. (2013). Optimal design of an automotive fan using the Turb'Opty meta-model. *Computers and Fluids*, 80(1), 207–213. <https://doi.org/10.1016/j.compfluid.2012.03.015>
- Canepa, E., Cattanei, A., Mazzocut Zecchin, F., Milanese, G., & Parodi, D. (2016). An experimental investigation on the tip leakage noise in axial-flow fans with rotating shroud. *Journal of Sound and Vibration*, 375, 115–131. <https://doi.org/10.1016/j.jsv.2016.04.009>
- Canepa, E., Cattanei, A., Moradi, M., & Nilberto, A. (2021). Experimental study of the leakage flow in an axial-flow fan at variable loading. *International Journal of Turbomachinery, Propulsion and Power*, 6(4). <https://doi.org/10.3390/ijtpp6040040>
- Canepa, E., Cattanei, A., & Neshat, M. A. (2023, January). *Cfd study of the leakage flow in low-speed axial-fan with rotating shroud*. European Conference on Turbomachinery Fluid Dynamics and Thermodynamics, ETC. <https://doi.org/10.29008/etc2023-215>
- Chen, L., Xie, H., Xu, J., Dai, R., & Chen, J. (2018). Experimental and numerical study on the performance of an axial fan with a Gurney flap. *Advances in Mechanical Engineering*, 10(10), 1–17. <https://doi.org/10.1177/1687814018803804>
- Chen, S., Gong, Y., & Zeng, C. (2022). Experimental investigation of hole-type bleed for active flow control in an axial compressor cascade with tip clearance. *Aerospace Science and Technology*, 128, 107790. <https://doi.org/10.1016/j.ast.2022.107790>
- Chen, S., Zhou, Z., Meng, Q., Wang, S., & Zhou, X. (2017). Experiment study of the winglet-cavity tip on the aerodynamic performance in a turbine cascade. *Proceedings of the Institution of Mechanical Engineers, Part A: Journal of Power and Energy*, 231(7), 676–685. <https://doi.org/10.1177/0957650917720560>
- Eberlinc, M., Širok, B., Dular, M., & Hočevár, M. (2009). Modification of axial fan flow by trailing edge self-induced blowing. *Journal of Fluids Engineering*, 131(11). <https://doi.org/10.1115/1.4000345>
- International Organization for Standardization. (2007). *Industrial fans - Performance testing using standardized airways*. (ISO 5801:2007).
- Magne, S., Moreau, S., & Berry, A. (2015). Subharmonic tonal noise from backflow vortices radiated by a low-speed ring fan in uniform inlet flow. *The Journal of the Acoustical Society of America*, 137(1), 228–237. <https://doi.org/10.1121/1.4904489>
- Moreau, S., & Sanjose, M. (2016). Sub-harmonic broadband humps and tip noise in low-speed ring fans. *The Journal of the Acoustical Society of America*, 139(1), 118–127. <https://doi.org/10.1121/1.4939493>
- Nadeau, S. (2005). *Integral tip seal in a fan-shroud structure*. Siemens VDO Automotive Inc., US Patent 56874990.
- Neuhaus, L., & Neise, W. (2007). Active control to improve the aerodynamic performance and reduce the tip clearance noise of axial turbomachines with steady air injection into the tip clearance gap. In R. King (Ed.), *Active Flow Control* (pp. 293–306). Springer Berlin Heidelberg. [https://doi.org/10.1007/978-3-540-71439-2\\_18](https://doi.org/10.1007/978-3-540-71439-2_18)
- Pereira, M., Ravelet, F., Azzouz, K., Azzam, T., Oualli, H., Kouidri, S., & Bakir, F. (2021). Improved aerodynamics of a hollow-blade axial flow fan by controlling the leakage flow rate by air injection at the rotating shroud. *Entropy*, 23(7). <https://doi.org/10.3390/e23070877>
- Piellard, M., Coutty, B., Le Goff, V., Vidal, V., & Pérot, F. (2014, June 1–16). *Direct aeroacoustics simulation of automotive engine cooling fan system: Effect of upstream geometry on broadband noise*. 20th AIAA/CEAS Aeroacoustics Conference. <https://doi.org/10.2514/6.2014-2455>
- Pogorelov, A., Meinke, M., & Schröder, W. (2016). Effects of tip-gap width on the flow field in an axial fan. *International Journal of Heat and Fluid Flow*, 61, 466–481. <https://doi.org/10.1016/j.ijheatfluidflow.2016.06.009>
- Qingyi, S., Haodong, X., Jian, C., & Jiangtao, Z. (2023).

- Experimental and numerical study on a new noise reduction design for a small axial fan. *Applied Acoustics*, 211, 109535. <https://doi.org/10.1016/j.apacoust.2023.109535>
- Rey, R. (1981). *Méthode générale de détermination d'un étage de turbomachine axiale de compression (fluide incompressible)*.
- Sarraf, C., Nouri, H., Ravelet, F., & Bakir, F. (2011). Experimental study of blade thickness effects on the overall and local performances of a controlled vortex designed axial-flow fan. *Experimental Thermal and Fluid Science*, 35(4), 684–693. <https://doi.org/10.1016/j.expthermflusci.2011.01.002>
- Sheng, C., & Zhao, Q. (2017). Numerical investigations of fan-in-wing aerodynamic performance with active flow control. *Journal of Aircraft*, 54(6), 2317–2329. <https://doi.org/10.2514/1.C034134>
- Wasilczuk, F., Flaszynski, P., Kaczynski, P., Szwaba, R., Doerffer, P., & Marugi, K. (2021). Air curtain application for leakage reduction in gas turbine shroud sealing. *Aerospace Science and Technology*, 112, 106636. <https://doi.org/10.1016/j.ast.2021.106636>
- Yadegari, M., & Bak Khoshnevis, A. (2020). Entropy generation analysis of turbulent boundary layer flow in different curved diffusers in air-conditioning systems. *European Physical Journal Plus*, 135(6). <https://doi.org/10.1140/epjp/s13360-020-00545-y>
- Yadegari, M., & Bak Khoshnevis, A. (2021). Investigation of entropy generation, efficiency, static and ideal pressure recovery coefficient in curved annular diffusers. *The European Physical Journal Plus*, 136(1), 69. <https://doi.org/10.1140/epjp/s13360-021-01071-1>
- Yadegari, M., Ommi, F., Karimian Aliabadi, S., & Saboohi, Z. (2024). Reducing the aerodynamic noise of the axial flow fan with perforated surface. *Applied Acoustics*, 215, 109720. <https://doi.org/10.1016/j.apacoust.2023.109720>